Fermi surface and quantum well states of V(110) films on W(110)

2007 J. Phys.: Condens. Matter 19 355005

(http://iopscience.iop.org/0953-8984/19/35/355005)

IOP PUBLISHING JOURNAL OF PHYSICS: CONDENSED MATTER

J. Phys.: Condens. Matter **19** (2007) 355005 (14pp) doi:10.1088/0953-8984/19/35/355005

Fermi surface and quantum well states of V(110) films on W(110)

Oleg Krupin[1,2], **Eli Rotenberg**[1] **and S D Kevan**[2]

[1] MS 6-2100, Advanced Light Source, Lawrence Berkeley National Laboratory, Berkeley, CA 94720, USA
[2] Department of Physics, University of Oregon, Eugene, OR 97403, USA

Received 29 September 2006, in final form 10 November 2006
Published 20 August 2007
Online at stacks.iop.org/JPhysCM/19/355005

Abstract

Using angle-resolved photoemission spectroscopy, we have measured the Fermi surface of V(110) films epitaxially grown on a W(110) substrate. We compare our results for thicker films to existing calculations and measurements for bulk vanadium and find generally very good agreement. For thinner films, we observe and analyse a diverse array of quantum well states that split and distort the Fermi surface segments. We have searched unsuccessfully for a thickness-induced topological transition associated with contact between the zone-centre jungle gym and zone-boundary hole ellipsoid Fermi surface segments. We also find no evidence for ferromagnetic splitting of any bands on this surface.

(Some figures in this article are in colour only in the electronic version)

1. Introduction

The electronic structure of thin metallic films is of enduring interest due to the variety of interesting properties that are impacted by their reduced dimensionality. The formation of quantum well states, for example, leads to oscillatory coupling between magnetic films and modulates the electron–phonon coupling, work function, and surface chemical reactivity [1–3]. Even in the absence of quantum well state formation, the interplay between surface and volume effects in metallic thin films can lead to unusual magnetic behaviours such as perpendicular magnetic anisotropy [4], surface magnetic moments on non-magnetic [5] or antiferromagnetic metals [6], and modification of magnetic periodicities in films [7, 8]. For example, the surfaces of vanadium, which is located just to the left of the magnetic 3d transition metals, have been proposed to exhibit surface magnetism [5]. With a well-defined Fermi surface that is a moderate perturbation of that of paramagnetic chromium, this metal and its alloys with chromium also provide useful coupling media in magnetic and spintronic structures [9]. Finally, through the 1970s and 1980s there was significant debate concerning the Fermi surface topology of bulk vanadium and niobium [10–17]. More recently, interest in the Fermi surface properties of vanadium has been renewed by the observation of large, positive variation

of the superconducting transition temperature with pressure, with T_c approaching 20 K at $P \sim 130$ GPa [18, 19]. Topological transitions in the Fermi surface have been suggested to explain these observations. Possibly topological transitions might also be induced by dimensional confinement in thin films, thereby providing an interesting approach to control superconductivity.

To address some of these issues, we have undertaken and report here a systematic study of the electronic structure and Fermi surface of V(110) thin films using angle-resolved photoemission (ARP). In the thick-film limit, our results compare favourably to existing band structure calculations and to bulk Fermiology data. We find that thinner films exhibit a diverse array of quantum well (QW) states that split and distort the Fermi surface. We compare the thickness periodicity of these QW states to measured vectors that span the Fermi surface. We find no evidence for a topological transition involving the jungle gym and hole ellipsoid structures of the bulk Fermi surface as a function of thickness. We also find no evidence for surface magnetism on our (110)-oriented films.

The next section of this paper explains our experimental and data analysis procedures. We then describe the Fermi surface segments in the thick- and thin-film limit, comparing our results to the literature where possible. We conclude with a brief discussion of avenues to pursue in the future to probe thin-film modifications of bulk electronic structure.

2. Experimental procedures

Experiments were performed at the Electronic Structure Factory on beamline 7.0.1 at the Advanced Light Source at Lawrence Berkeley National Laboratory. Our procedures were very similar to those described previously [8, 20]. V(110) films were grown on clean W(110) by room-temperature evaporation followed by rapid annealing to ∼800 K. Despite the sizable lattice mismatch between vanadium and tungsten of ∼4%, we find that this procedure produces high-quality epitaxial films with sharp low-energy electron diffraction beams. Unlike Cr/W(110), where the lattice mismatch is more than twice as large [8], we are able to produce continuous films down to monolayer thickness. In most cases, films were deposited with a wedge-shaped thickness profile, typically with $0 \leqslant d \leqslant 15$ nm, over a distance of typically 5 mm. This is much larger than the 50 μm focal spot of the soft x-ray photon beam used in our photoemission experiments so that the thickness could be selected and controlled as desired. The focal spot is also smaller than the average V(110) monolayer terrace width due to the wedge angle of 70 μm. After preparation, the films were transferred in vacuum onto a liquid-He-cooled sample goniometer for ARP measurements over a temperature range of $20\ \text{K} < T < 300\ \text{K}$. Thin films displayed both excellent low-energy electron diffraction patterns and strong quantization of bulk states having significant perpendicular dispersion, indicating high-quality vanadium–vacuum and the vanadium–tungsten interfaces. The base pressure of our vacuum system was typically $\sim 2 \times 10^{-11}$ Torr, though the pressure increased by about an order of magnitude during vanadium evaporation.

The Gammadata R4000 electron energy analyser employed in these experiments was fixed in space in the horizontal plane defined by the incident photon beam and polarization directions at an angle of 30° to the latter. This analyser measures in parallel a polar angular range of ∼30° and an energy window dependent on the analyser pass energy. Most of our data sets start with (energy, angle) band maps, produced directly by this analyser, though often these are transformed through image analysis and interpolation to produce more useful cuts through momentum space. In particular, with the necessary variation of photon energy, our data sets often include components both parallel ($k_\parallel$) and perpendicular ($k_\perp$) to the surface plane. These data sets can be interpolated to produce planar slices through k-space, an

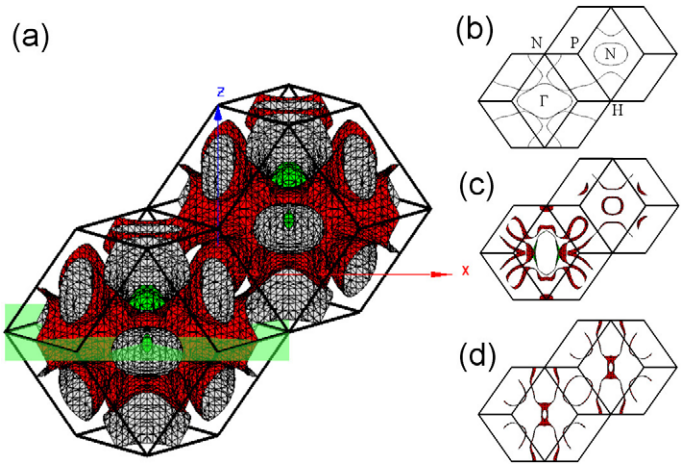

Figure 1. (a) Calculated vanadium Fermi surface, based on the data in [25], plotted in the first two bcc Brillouin zones. The (green) Γ-centred electron pocket is barely visible inside the (red) extended jungle gym sheet. The figure shows N-centred hole ellipsoids being connected to the jungle gym, which is at odds with these and other [12] measurements as well as recent first-principles theory [26]. The (green) plane cuts the Γ–N–P–H plane of the bcc Brillouin zone normal to the V(110) axis. Panel (b) shows a slice through the $k_\perp = (2\pi/a)(000)$ and $k_\perp = (2\pi/a)(1/2, 1/2, 0)$ planes, which are simply offset by $k_\parallel = (2\pi/a)(1/2, 1/2, 1)$. Similarly, panels (c) and (d) show slices $(1/8, 1/8, 0) = (2\pi/a)(3/8, 3/8, 0)$ and at $k_\perp = (2\pi/a)(1/4, 1/4, 0)\mathbf{k}_\perp = (2\pi/a)$, respectively.

important feature when comparing to calculations and other Fermi surface measurements which are often reported only in symmetry planes. While the parallel component of momentum is conserved in ARP, it is well known that other information or approximations are needed to deduce the perpendicular component [21–23]. Our interpolations make the simplest possible approximation: that is, that the final state is characterized by a free electron dispersion relation with an inner potential chosen to force various symmetries on the resulting images [24]. At the fairly high photon energy range used in these experiments (80–200 eV), this approximation is generally successful, at least over moderate ranges of momentum. We return to this issue in the discussion section 3.1.

The angular flexibility of our experiments was provided primarily through rotations facilitated by the sample goniometer. Three precision angular degrees of freedom were available: the polar angle of the surface normal relative to the energy analyser (θ), azimuthal angle of rotation about the normal (ϕ), and tilt of the normal out of the horizontal plane (β). All of these angles are continuously driven with stepper-motors and are under computer control. The precision is typically 0.1°.

3. Results and discussion

3.1. Fermi surface in the Γ*–N–P–H plane*

The calculated Fermi surface for bulk vanadium is shown in figure 1, along with the body-centred cubic (bcc) Brillouin zone [25]. The Fermi surface consists of three parts that correspond to better-known segments of the group VIB metal Fermi surface after addition of a single hole per atom [11]. There is first an electron pocket centred at the zone centre Γ-point, a remnant of the larger chromium electron octahedron. Second, there is an extended

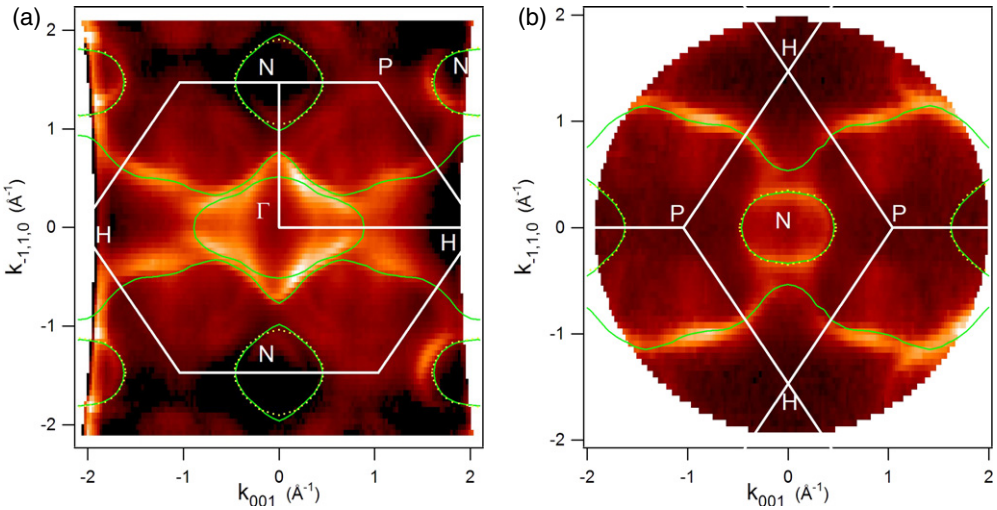

Figure 2. (a) ARP intensity map at $k_\perp = (2\pi/a)(220) \equiv k_\perp = 0 =$ the Γ–N–P–H plane in the reduced bcc Brillouin zone. Data were collected at the Fermi level from a 20 nm thick film. Bright regions correspond to bands crossing E_F, and thus to sections of the bulk Fermi surface. Curves were produced by a recent LDA + U calculation [26], while the circles are the results from a de Haas–van Alphen measurement of bulk vanadium [10]. The match between our measurement and these other results is generally very good near the middle of the image, though less good near the periphery. (b) Similar intensity map for $k_\perp = (2\pi/a)(5/2, 5/2, 0) \equiv (2\pi/a)(1/2, 1/2, 0)$ in the reduced zone scheme. These data sample the same plane as in panel (a), except that it has been translated by $k_\parallel = (2\pi/a)(1/2, 1/2, 1)$ so the section of the ellipse centred at N is more readily visible.

jungle gym (JG) structure that results from the merging of the hole octahedra centred at the H-points in chromium. Similar structures in all the group VB metals support open Fermi surface orbits, a feature that is distinct from the group VIB metals. Finally, there are hole ellipsoids centred at the N-points. These are larger than the analogous ellipsoids in chromium due to the smaller electron count in vanadium. Controversy has existed as to whether or not these ellipsoids are large enough to contact the JG through small necks along the Σ-axes. Indeed, the web site that is the source of figure 1 suggests that these necks exist and that the segments are therefore joined, though experiments and modern calculations now generally agree that the correct topology has them separated [11–14, 16, 18, 26].

Figure 2(a) shows an ARP intensity map of a V(110) film of thickness 20 nm, at a temperature of 25 K, and sampling states at the Fermi level E_F. As discussed above, the image has been interpolated from a larger data set to produce a slice through the Γ–N–P–H plane of the bcc Brillouin zone. The data were collected over a range of photon energy between 80 and 200 eV, and over angular ranges of typically 30° in orthogonal directions: the polar angle θ provided by the R4000 analyser and the tilt angle β provided by sweeping the sample goniometer. The interpolated plane corresponds to the reciprocal lattice vector $\mathbf{K} = (2\pi/a)(2, 2, 0)$. This in turn sets the perpendicular component of the wavevector, $k_\perp = 5.88$ Å^{-1}, which by reciprocal lattice symmetry is equivalent to $k_\perp = 0.0$ Å^{-1}. To infer the perpendicular component, we have numerically 'scanned' the $k_\perp$ plane through the data set and searched for the symmetry plane with contours that most closely match the experiment. At high energy, this is roughly equivalent to varying the inner potential so as to locate the observed symmetry plane at the known value of $k_\perp$ [22, 23].

Bright portions of this image correspond to regions of k-space where a band crosses the sampled energy. Since this energy is set to E_F in this figure, the photoemission data provide a direct image of a cut through the underlying Fermi surface. The curves displayed over the image in this figure are slices of the vanadium Fermi surface calculated using the LDA + U approximation [26]. There is generally very good qualitative correspondence between the calculated and measured Fermi surface, with features from the zone centre electron pocket, the jungle gym, and the ellipsoid being readily apparent. Near the middle of the image, which corresponds experimentally to electrons photoemitted near the surface normal ($k_\parallel \sim 0$), there is good quantitative agreement between experiment and theory, particularly for the zone-centre electron pocket and the JG.

Further away from zone centre, the agreement is less good, particularly for the ellipsoidal hole pockets near the N $= (2\pi/a)(1/2, 1/2, 1)$ point. One might question the validity of the free-electron final state used to scale and interpolate this image; such a final state may not be globally valid with fixed electron mass and inner potential. However, this effect would lead to interpolations that do not slice precisely through middle of the ellipsoids at the N-points. The resulting Fermi slices would be the wrong size, but they should remain closely centred at the correct locations in k-space. This is at odds with our interpolated images, which exhibit segments that are slightly displaced from the N-points. We believe the observed asymmetry to be an experimental artefact. Band maps from the Scienta R4000 analyser become slightly distorted at higher emission angles. We have normalized these nonlinearities as well as we can, but in figure 2(a), the asymmetry remains, particularly when comparing features at widely separated angles. The offset exists mostly in the [001] direction and to a lesser degree in the $[\bar{1}, 1, 0]$ direction. Our normalization is imperfect, but the distortion in the $[\bar{1}, 1, 0]$ direction, which is scanned mechanically rather than imaged electronically with the Scienta analyser, suggests that stray electric and magnetic fields probably also contribute to the remaining asymmetry.

Rather than address these distortions directly, we can make good progress by scanning $k_\perp$ through other symmetry planes where, for example, the N-point is located at normal emission. An obvious choice is $k_\perp = (2\pi/a)(5/2, 5/2, 0)$, or $k_\perp = 7.35$ Å^{-1}, which samples directly the bcc zone boundary rhombus with N at its centre. Such an image is presented in figure 2(b), and the same three Fermi surface segments are easily observed. Note that this image actually samples the same symmetry plane as in panel (a), except that it is translated by $k_\parallel = (2\pi/a)(1/2, 1/2, 1)$. The section of the N-point hole ellipsoid is now clearly visible about $k_\parallel = 0$, as is the extension of the JG between the Γ- and N-points. The Γ-centred electron pocket is now visible at higher $k_\parallel$, though somewhat distorted. The agreement between the calculated and experimental elliptical and JG segments near the N-point is now very good.

A geometrical factor increases the precision of our measurement of Fermi surface sections in a symmetry plane. The component of band velocity perpendicular to the surface vanishes in this geometry due to symmetry. For this reason, the Fermi surface sections will be stable to second order in any offset of $k_\perp$ from the symmetry plane. Moreover, photoemission line widths of 3D states are minimized in this geometry [22, 24, 27], thereby further increasing the accuracy of the measurement. While photoemission probes 3D electronic structure, it works best when measuring extremal slices of 3D Fermi surfaces—similar to bulk de Haas–van Alphen techniques, though for very different reasons.

The dotted contours in figures 2(a) and (b) present the result from bulk de Haas–van Alphen measurements of the elliptical hole pocket [10]. The accord between our experiment, the de Haas–van Alphen results, and the LDA + U calculation is very good. Corresponding Fermi surface ellipsoids in chromium are thought to play a role in mediating magnetic interactions in multilayers [9], and to the extent that vanadium is used in a similar fashion, these data

Table 1. Measured and calculated nesting vectors associated with the N-point ellipsoids in vanadium in four different directions.

k-space line	This study (Å^{-1})	Bulk measurement [14] (Å^{-1})	Calculation [26] (Å^{-1})
G = H–N–H	0.65	0.70	0.67
D = P–N–P	0.82	0.95	0.92
Σ = Γ–N–Γ	0.72	0.86	0.98
N–N	0.75		

can be used to make quantitative predictions. These results, combined with the pronounced quantum well states associated with the ellipsoids presented in the following section, suggest that vanadium is a very good magnetic coupling agent. We have been unable to find experimental data in the literature using traditional Fermiology techniques for the Γ-centred electron pocket and the JG Fermi surface structures. This is likely a reflection of the difficulty of reconstructing the complicated, multi-segmented 3D Fermi surface from measurements of extremal areas derived from magneto-oscillation data [10, 12] and momentum densities from positron annihilation results [15, 16]. By contrast, ARP measurements produce symmetry sections directly.

3.2. Fermi surface in intermediate planes

Our measurements in the Γ–N–P–H plane of the bcc Brillouin zone offer a good calibration of the plane wave state used to calculate $k_\perp$. Using this we can produce by interpolation reasonably accurate Fermi surface sections at all $k_\perp$. In figure 3, for example, we show additional images at $k_\perp$ values, reduced to the first Brillouin zone, of (a) $(2\pi/a)(1/8, 1/8, 0)$, (b) $(2\pi/a)(1/4, 1/4, 0)$, and (c) $(2\pi/a)(3/8, 3/8, 0)$. Lacking both experimental data and first-principles calculations with which to compare our results for the Fermi surface in these planes, we simply overlap the Fermi surface calculated using the semiempirical code of Papaconstantopoulos [28]. This code is based on first-principles APW bands calculated in the local density approximation. Such calculations often need to be adjusted slightly to obtain a good match to experimental Fermi surface results [14]. In the present case, the semiempirical results are nearly identical to those of the LDA + U calculation [26] for the JG and electron pockets in the Γ–N–P–H plane. As with other LDA calculations for group VB and VIB metals, the predicted sizes of the elliptical hole segments are systematically larger than experimental values. This generic problem contributed significantly to the discourse concerning the existence of necks connecting the ellipsoids to the jungle gym.

Given these uncertainties and those mentioned above in treating our experimental results, we discuss these results mostly in terms of their qualitative match to the calculation. In figure 3(a), the section of electron pocket is quite well reproduced, in a section where its overlap with the JG is less serious than in the symmetry plane. The faint curved segments centred at $k_{001} \sim k_{1\bar{1}0} \sim 1$ Å^{-1}, in panel (a) as well as in panels (b) and (c), correspond to slices through the hole ellipsoid at N = $(2\pi/a)(0, 1/2, \pm 1/2)$ and $(2\pi/a)(1/2, 0, \pm 1/2)$. In panel (b), the image slices through the middle of these ellipsoids which are therefore more pronounced. The jungle gym is less well defined in this plane, though if one compares this structure in figures 2(a) and (b), the result in panel (b) is a plausible interpolation. Finally, in panel (c), the slices through the $(2\pi/a)(0, 1/2, \pm 1/2)$ and $(2\pi/a)(1/2, 0, \pm 1/2)$ ellipsoids have again decreased in size while that through the $(2\pi/a)(1/2, 1/2, 1)$ ellipsoid has appeared, the JG has nearly been reconstituted as a coherent structure, and the zone-centre intensity has significantly reduced intensity.

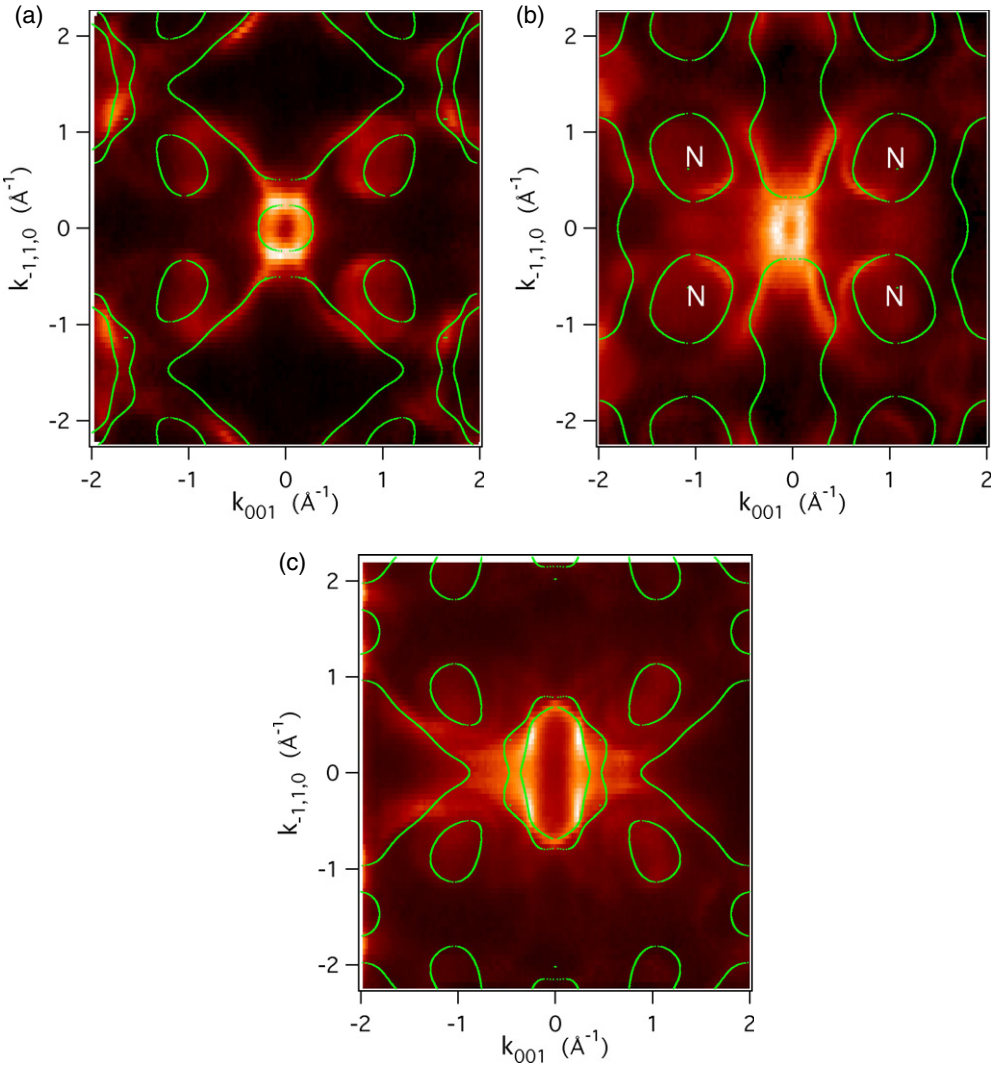

Figure 3. ARP intensity maps at intermediate planes (a) $k_\perp = (2\pi/a)(1/8, 1/8, 0)$, (b) $(2\pi/a)(1/4, 1/4, 0)$, and (c) $(2\pi/a)(3/8, 3/8, 0)$ in the reduced zone scheme. The curves in this case are produced by the semiempirical band structure routine of Papaconstantopoulos [28].

The data from figures 2(a), (b), and 3(b) allow us to measure the spanning vectors of the ellipsoidal Fermi surface segments in four different directions. These are given in table 1, where they are compared to bulk Fermi surface measurements [14] and to the LDA + U calculation [26].

3.3. Thin-film quantum well states

Precise characterization of quantum well states in the sp bands of metals on both metal and semiconductor substrates is now fairly common [1, 2, 29–33]. By contrast, observation of QW states in primarily d-like states in transition metal films remains unusual [31]. Nonetheless, we observe many QW states with significant 3d character in thin vanadium films on W(110).

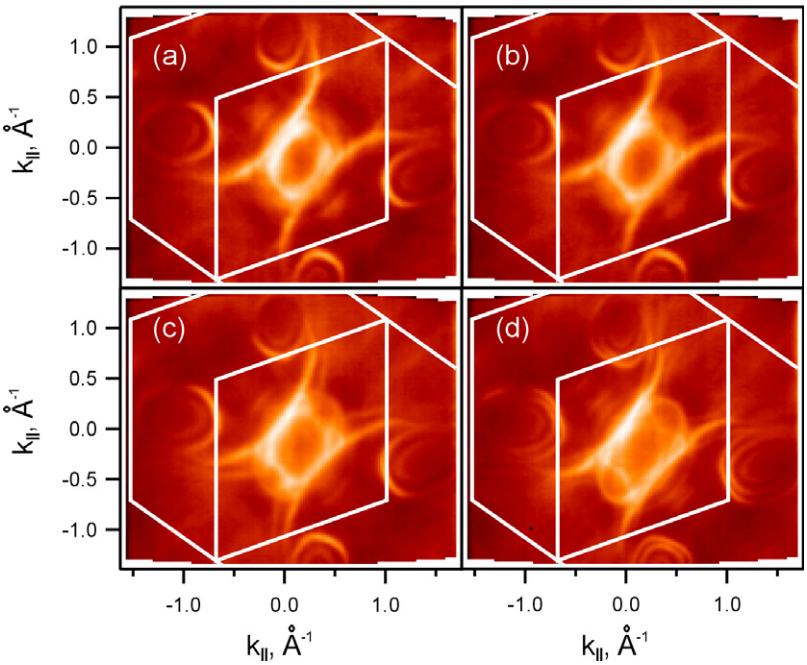

Figure 4. Fermi level ARP intensity maps at constant photon energy = 100 eV at four different values of film thickness: (a) 8 Å, (b) 9 Å, (c) 11 Å, and (d) 24 Å. 3d-character quantum well states associated with the ellipsoids in the plane $k_\perp = (2\pi/a)(1/4, 1/4, 0)$ and the jungle gym are readily apparent. Many other weaker QW states are also visible near the zone centre.

A good example is given in figure 4, which shows maps collected at the Fermi level at $h\nu =$ 100 eV for four different film thicknesses. These maps were collected at fixed photon energy and thus probe spherical rather than planar cuts through k-space. The Brillouin zone boundaries presented in the figures include both the $k_\perp = (2\pi/a)(0, 0, 0)$ and $k_\perp = (2\pi/a)(1/2, 1/2, 0)$ planes and are for reference only. A total of four closed, approximately elliptical contours are visible surrounding the N $= (2\pi/a)(0, 1/2, \pm 1/2)$ and $(2\pi/a)(1/2, 0, \pm 1/2)$ points as well as several other structures associated with the jungle gym. The sizes and intensities of these contours depend on the photon energy and film thickness—hallmarks of QW states observed with photoemission [1, 29, 30, 32]. The fact that quantum well states are intrinsically two dimensional justifies our use of a spherical rather than a planar cut through k-space. We present in figure 5(a) a map at a thickness of 11 Å. Figure 5(b) displays the thickness dispersion of the quantum well states at the Fermi level along the double-arrow line indicated in panel (a).

That the QW states for the ellipsoid and parts of the JG are so pronounced is probably caused by a large projected gap in the W(110) substrate electronic structure. This is shown graphically in figure 6, where we plot the calculated tungsten band structure (shaded region) projected onto the W(110) surface Brillouin zone (dotted lines) [28]. We also plot the calculated slice through the vanadium Fermi surface in the relevant plane, $k_\perp = (2\pi/a)(1/4, 1/4, 0)$, and the V(110) bulk Brillouin zone boundary (solid lines). In the first W(110) surface and V(110) bulk Brillouin zones, the elliptical and portions of the JG segments lie in a large projected band gap. This situation favours good localization of the QW states, since they cannot 'leak' into the tungsten substrate. An obvious complication is the 4% difference in lattice constant between vanadium and tungsten, which leads to different Brillouin zone dimensions for the

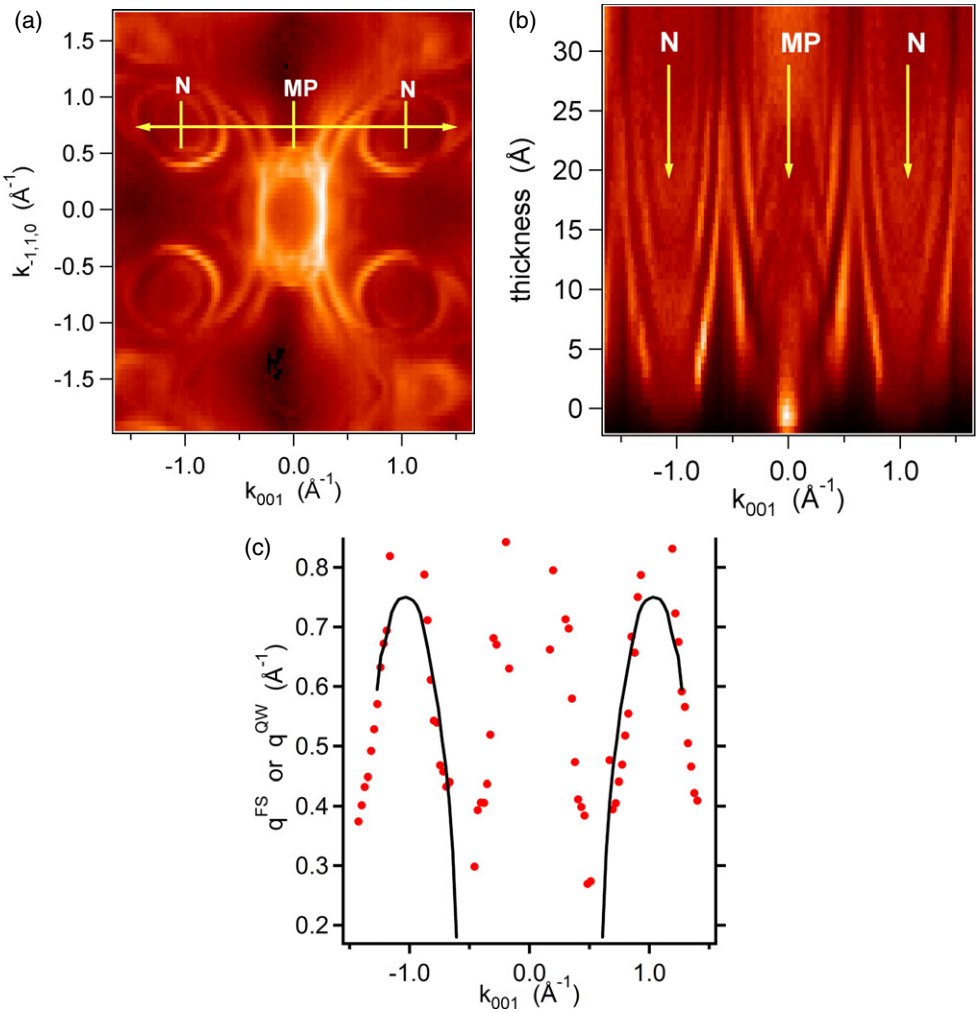

Figure 5. (a) Fermi map at a thickness of 11 Å at a photon energy of 100 eV. (b) ARP intensity map along the double-arrow line in panel (a) as a function of film thickness. Dispersion of the QW states with thickness is readily observed. (c) The filled circles denote the QW state thickness periodicity, $2\pi/\Delta d$, where Δd is the thickness interval, at constant $k_{\|}$, over which the intensity repeats. The solid curves indicate the periodicity expected from the Fermi surface section in 3(b), as explained in the text.

film and substrate, as shown in figure 6. This intrinsic incommensurability means that the vanadium states will be coupled to tungsten states in higher Brillouin zones. However, the coupling through such interface Umklapp processes is generally weak. Our results tend to confirm that. We observe QW states associated with most of the vanadium bands in thin films, but these are usually less dramatic than those which lie in the W(110) projected band gap. For example, a few faint QW states associated with the N $= (2\pi/a)(1/2, 1/2, 0)$ points are visible surrounding the intense features near the middle of the images in figure 4. To the extent that these well-confined QW states can be translated into magnetic heterostructures, vanadium films should provide an interesting medium to couple magnetic interactions over extended distances through an RKKY-like interaction [30, 32, 33].

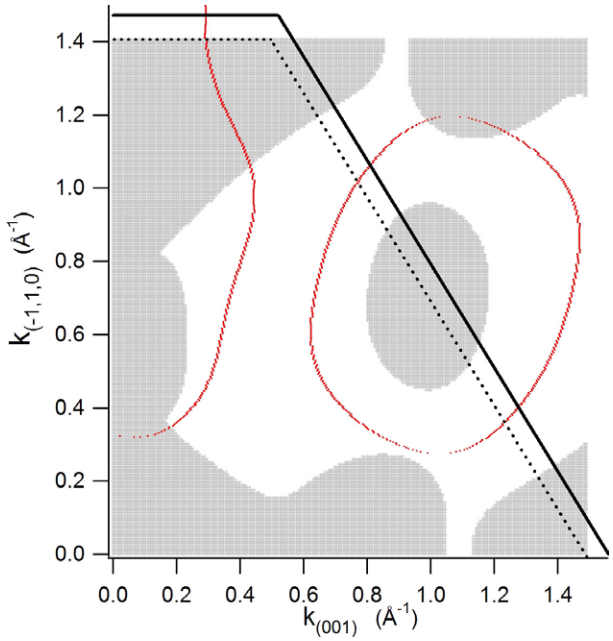

Figure 6. The shaded region presents the calculated [28] bulk tungsten Fermi surface projected onto the W(110) surface Brillouin zone denoted by the dashed line. The curve presents a slice through the vanadium Fermi surface at $k_\perp = (2\pi/a)(1/4, 1/4, 0)$, corresponding to the results in figures 4 and 5. Note that the calculation overestimates the size of the ellipsoidal hole pocket by 10–15%. The boundary of the bulk vanadium bcc Brillouin zone is given by the solid line. QW states are most pronounced within the projected band gap in the W(110) Fermi surface.

To analyse these QW states more completely, we first consider in detail the states associated with the ellipsoidal Fermi surface segments discussed above. The thickness period of such quantum well states can be predicted with the Bohr–Sommerfeld quantization condition [1, 29, 30, 32, 34]. To form a stationary state, the QW wavefunction must accumulate a total phase that is an integral (N) multiple of 2π in a round trip through a film of thickness d:

$$2k_\perp(E)d + \Phi(E) = 2\pi N, \tag{1}$$

where Φ is a phase shift accumulated in scattering off the two interfaces. These ellipsoids present a slightly more complex situation than in some previous studies for two reasons. First, we are considering hole pockets near the Brillouin zone boundary. In this case, the perpendicular wavevector is an effective wavenumber that is measured from the Brillouin zone boundary N-point, and the resulting quantum well 'wavefunction' is in reality that of an envelope function that modulates a more rapidly oscillating Bloch function [1, 29, 32]. The second complexity is that the symmetry elements of the N-points in this k_{110} section include only a two-fold rotation, so $E(+k_\perp)$ is not equal to that $E(-k_\perp)$. That is, the phase accumulated by a QW wavefunction approaching the W–V interface is different from the phase it accumulates approaching the V–vacuum interface. In this case, the quantization condition changes to

$$k_\perp^+(E)d + k_\perp^-(E)d + \Phi(E) = 2\pi N, \tag{2}$$

where $k_\perp^+(E)$ and $k_\perp^-(E)$ are these two wavevectors.

Equation (2) indicates that, at a given energy E—the Fermi level, for example—consecutively indexed QW states will have a thickness period $\Delta d = d(N+1) - d(N) =$

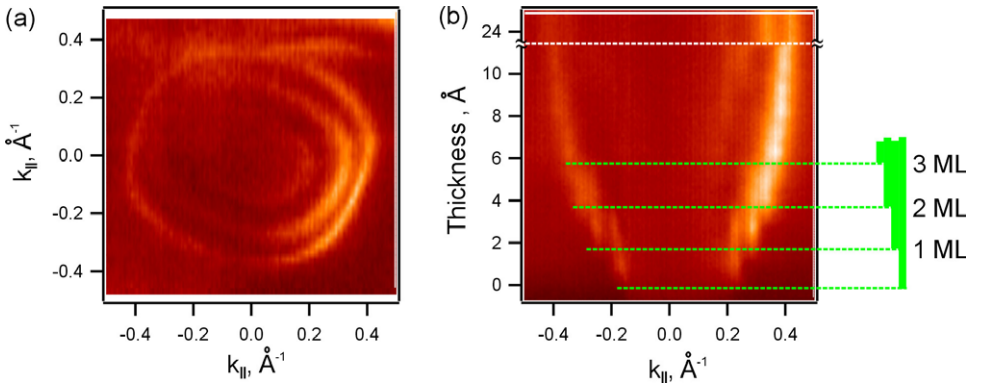

Figure 7. (a) ARP intensity map collected at the Fermi level focusing on the QW states surrounding the N-point ellipsoid at $(2\pi/a)(0, 1/2, \pm 1/2)$. Panel (b) shows the thickness dispersion of the ellipsoidal Fermi surface segments, as in figure 5(b), except that the data were collected from a higher-quality film. Note the formation of stripes of intensity at constant $k_\parallel$ for films a few monolayers thick. The periodicity of these stripes is 1 monolayer, and they are associated with the Fermi wavevectors of the ellipsoid in the 1–3 monolayer limit, as shown schematically on the right.

$2\pi/(k_\perp^+ + k_\perp^-)$. This periodic behaviour is readily visible in figure 5(b). In turn, the quantity $q_|^{\mathrm{QW}}(k_\parallel) = 2\pi/[d(N+1) - d(N)]$ is predicted to be equal to the vector, $q^{\mathrm{FS}}(k_\parallel) = k_\perp^+ + k_\perp^-$, which spans the underlying segment of the bulk Fermi surface at the $k_\parallel$ being considered. With perfect thickness calibration, such studies provide an independent way to determine the Fermi surface dimensions. Since our thickness calibration is not perfect, we tend to associate the measured periods with a relevant, preferably measured spanning vector, and then use this association to calibrate the angle of our thickness wedge.

We extracted the thickness periodicity $q_|^{\mathrm{QW}}(k_\parallel)$ by fitting the data in figure 5(b) along lines of constant k_{001}. A careful examination of the Fermi surface in figure 1 indicates that the relevant Fermi surface spanning vectors are associated with lines parallel to the $[\bar{1}, 1, 0]$ axis in figure 3(b)—a direction that is equivalent to the [110] axis normal to the film plane. We fitted the elliptical contour in figure 3(b) and extracted the spanning vectors, $q^{\mathrm{FS}}(k_\parallel)$. Figure 5(c) plots the derived values of $q^{\mathrm{FS}}(k_\parallel)$ (black curves) and $q^{\mathrm{QW}}(k_\parallel)$ (red points) as a function of $k_\parallel$ along the [001] direction, the direction indicated by the double arrow in figure 5(a). Without tuning our thickness calibration at all we find fairly good accord between these two. We do not trust the measurements near the N-points in this fitting procedure, both because the films are very thin and are thus endowed with significant strain and also because the intensity of the QW states is very low.

The above analysis indicates that the thickness dispersion of the ellipsoidal QW states can be well understood within the confines of the simple phase accumulation model involving intraband nesting vectors. However, a closer examination of figure 5(b) suggests that additional structure might exist in few-monolayer-thick films. As indicated in figure 7, our highest-quality films reveal that this structure takes the form of constant $k_\parallel$ stripes in the thickness dispersion data. These stripes are associated with the first few atomic vanadium layers, as demonstrated in figure 7(b). These results confirm our film thickness calibration and offer a detailed, layer-by-layer view of the Fermi surface evolution.

The behaviour of the QW states associated with the JG Fermi segment is qualitatively similar though more complex than those associated with the ellipsoids. These overlap other bulk and quantum well states close to the mirror plane at $k_{001} = 0$ in figure 5(b). This

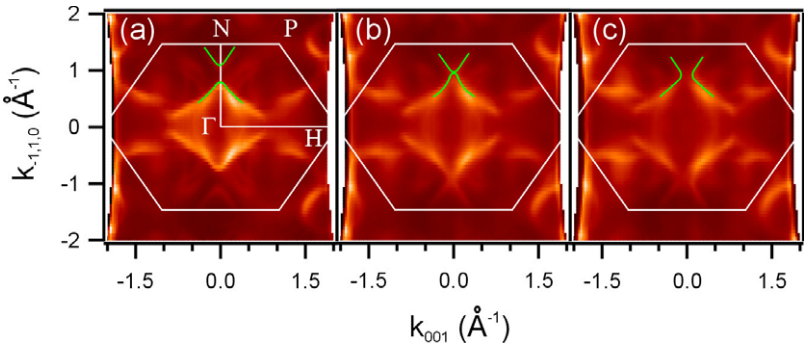

Figure 8. ARP intensity maps collected from a 20 nm thick film at $T = 25$ K at $k_\perp = (2\pi/a)(220)$, at binding energies of (a) 0 meV, (b) 160 meV, and (c) 270 meV. Note the merging of the contours associated with the hole ellipsoids and the jungle gym along the Γ–N = Σ axes, corresponding to a topological transition that occurs when the sampled energy moves through a band minimum along the Σ-line.

hybridization apparently causes the JG QW states to reverse the direction of dispersion near the mirror plane. We have not tried to understand this behaviour in detail. Also, we are unable to fit the JG QW thickness dispersion within the context of the simplest phase analysis model. A quick examination of figure 3(b), for example, suggests that the most likely nesting vector for the JG varies rapidly with k_{001} and is generally nearly twice as large as the nesting vector for the ellipsoids. However, the observed JG thickness periodicity in figures 5(b) and (c) is comparable to that of the ellipsoids. Probably the close proximity of other segments of the vanadium Fermi surface renders the simplest phase analysis model discussed above inadequate. These results will be the subject of further studies.

As noted above, we observe many other weaker QW states for this system. We have not attempted to make a detailed analysis of these, since they likely will have a smaller impact on thin film properties.

3.4. Further discussion

We now analyse our results in terms of some of the interesting issues presented in section 1. First, the results in figure 2(a) confirm directly that there is no neck connecting the hole ellipsoid and the jungle gym segments of the vanadium Fermi surface. These necks would connect these sections along the Γ–N = Σ line, near $k_{1\bar{1}0} = \pm 0.8$ Å^{-1}. The hole pocket contours centred at the $(2\pi/a)(\pm 1/2, 1/2, 0)$ N-points in these regions have small but measurable intensity, and are clearly separated from the more intense jungle gym segments. The measured separation between these segments along the Σ line is ∼0.4 Å^{-1}, in good agreement with recent calculations [26]. Moreover, despite the distortion of the Fermi surface segments caused by quantum well formation discussed in the previous section, nothing resembling a neck connecting these two sheets at E_F is observed at any thickness. It is apparently not possible to induce a topological transition by controlling the film thickness, at least for this (110) film orientation. To confirm and illuminate this conclusion further, we show in figure 8 ARP intensity maps in the $k_\perp = (2\pi/a)(1/4, 1/4, 0)$ plane as a function of binding energy for a 20 nm thick film where QW states are not observed. The hole and jungle gym segments both grow as the binding energy increases, and merge at $E_B < 150$ meV. This connection is determined by the maximum binding energy of a Σ_1-symmetry band that disperses slightly below E_F along the Γ–N direction. In the LDA + U calculation [26], this maximum binding

energy is ∼70 meV, which is slightly less than the binding energy at which we observe the topological transition.

Predictions of possible magnetic structures localized at vanadium surfaces and on vanadium particles [35] that were made some time ago for V(100) remain controversial [36] V(110), being the closest-packed bcc surface, is less likely to exhibit ferromagnetism than either other low-index surface. Our results do not exhibit any features that obviously indicate a magnetic ground state at any thickness down to a single monolayer. In the thick-film limit, the number of Fermi contours is in accord with expectations, and none of the contours appear to be split by an exchange interaction. We have made measurements as a function of temperature, and down to 25 K, only smooth changes in intensity are observed. While we observe many splittings due to quantum well formation, no temperature-dependent splittings that might indicate an electronic phase transition have been located. We have also undertaken a cursory search for magnetic ground states in V(100) films grown on a Mo(100) substrate, with similar negative results.

We have not attempted to observe modulations of the electron–phonon coupling, work function, and surface chemical reactivity that have been associated with quantum well formation in other systems [2, 3]. Given the large number of quantum well states observed on V(110), and their substantial amplitude in terms of photoemission intensity, it is likely that searches for such modulations would meet with success.

4. Concluding remarks

We have presented results for the Fermi surface segments of V(110) films on a W(110) substrate. While we have not observed exotic behaviours like surface magnetism or thickness-induced topological transitions in the Fermi surface, our results nonetheless suggest some fruitful future directions for investigation. Vanadium and chromium–vanadium alloys are common coupling layers in magnetic films, and our results provide benchmarks for spatial periodicities that might be observed in these. Our results can be extended to alloys of these two metals, in which case topological transitions would certainly be observed with possibly unusual behaviours resulting. Our results also provide a basis for comparison in the search for surface magnetism on other low-index and vicinal vanadium surfaces. Finally, the strength of the observed quantum well states suggests that finite-size effects might influence a variety of other surface properties such as the work function, electron–phonon interaction, and chemical reactivity.

Acknowledgments

This work was supported by the US DOE under grant DE-FG02-04ER46158. The Advanced Light Source is operated under US DOE contract DE-AC03-76SF00098 at Lawrence Berkeley National Laboratory.

References

[1] Chiang T-C 2000 *Surf. Sci. Rep.* **39** 181
[2] Luh D-A *et al* 2001 *Science* **292** 1131
[3] Paggel J J *et al* 2002 *Phys. Rev.* B **66** 233403
Guo Y *et al* 2004 *Science* **306** 1915
Bao X-Y *et al* 2005 *Phys. Rev. Lett.* **95** 247005
[4] Pommier J *et al* 1990 *Phys. Rev. Lett.* **65** 2054

Garcia P F 1988 *J. Appl. Phys.* **63** 5066
[5] Ohnishi S, Fu C L and Freeman A J 1985 *J. Magn. Magn. Mater.* **50** 161
Khalifeh J 1997 *J. Magn. Magn. Mater.* **168** 25
Homouz D M and Khalifeh J M 1996 *J. Magn. Magn. Mater.* **153** 355–8
Robles R *et al* 2001 *Phys. Rev.* B **63** 172406
Dreyesse H *et al* 1995 *Europhys. Lett.* **27** 165
[6] Klebanoff L E *et al* 1984 *Phys. Rev.* B **30** 1048
Klebanoff L E *et al* 1985 *Phys. Rev.* B **31** 6379
Klebanoff L E *et al* 1985 *Phys. Rev.* B **32** 1997
[7] Zabel H 1999 *J. Phys.: Condens. Matter* **11** 9303
Fishman R S and Shi Z-P 1998 *J. Phys.: Condens. Matter* **10** L277
Fishman R S and Shi Z-P 1999 *Phys. Rev.* B **59** 13849
Fishman R S 2000 *J. Phys.: Condens. Matter* **13** R235
Meersschaut J *et al* 1995 *Phys. Rev. Lett.* **75** 1638
Fritzsche H *et al* 2003 *Eur. Phys. J.* B **36** 175
Fritzsche H *et al* 2002 *Phys. Rev.* B **65** 144408
[8] Rotenberg E *et al* 2005 *New J. Phys.* **7** 1142005
[9] Hughes R J *et al* 2004 *Phys. Rev.* B **69** 174406
[10] Phillips R A 1971 *Phys. Lett.* A **36** 361
[11] Mathiess L F 1965 *Phys. Rev.* **139** A1893
[12] Parker R D and Halloran M H 1974 *Phys. Rev.* B **9** 4130
[13] Papaconstantopoulos D A, Anderson J R and McCaffrey J W 1972 *Phys. Rev.* B **5** 1214
Elyashar N and Koelling D D 1977 *Phys. Rev.* B **15** 3620
Crabtree G W *et al* 1979 *Phys. Rev. Lett.* **42** 390
Manuel A A 1982 *Phys. Rev. Lett.* **49** 1525
[14] Major Zs *et al* 2004 *J. Phys. Chem. Solids* **65** 2011–6
[15] Pecora L M *et al* 1988 *Phys. Rev.* B **37** 6772
[16] Singh A K *et al* 1985 *J. Phys. F: Met. Phys.* **15** 2375
[17] Laurent D G, Wang C S and Callaway J 1978 *Phys. Rev.* B **17** 455
[18] Tse J S *et al* 2004 *Phys. Rev.* B **69** 132101
[19] Louis C N and Iyakutti K 2003 *Phys. Rev.* B **67** 094509
Ishizuka M, Iketani M and Endo S 2000 *Phys. Rev.* B **61** R3823
Suzuki N and Otani M 2002 *J. Phys.: Condens. Matter* **14** 10869
[20] Schäfer J *et al* 1999 *Phys. Rev. Lett.* **83** 2069
Rotenberg E and Kevan S D 1998 *Phys. Rev. Lett.* **80** 2905
[21] Kevan S D 1992 *Angle-Resolved Photoemission* (Amsterdam: Elsevier)
Hüfner S *et al* 1999 *J. Electron Spectrosc.* **100** 191
Hüfner S 1995 *Photoelectron Spectroscopy* (Berlin: Springer)
[22] Himpsel F J 1985 *Adv. Phys.* **32** 1
[23] Plummer E W and Eberhardt W 1982 *Advances in Chemical Physics* vol 49 (New York: Wiley)
[24] Thiry P *et al* 1979 *Phys. Rev. Lett.* **43** 82
[25] Choy T S http://www.phys.ufl.edu/fermisurface/
Choy T-S *et al* 2000 *Bull. Am. Phys. Soc.* **45** L36
[26] Tokii M and Wakoh S 2003 *J. Phys. Soc. Japan* **72** 1476
[27] Eastman D E, Knapp J A and Himpsel F J 1978 *Phys. Rev. Lett.* **41** 825
Tersoff J and Kevan S D 1983 *Phys. Rev.* B **28** 4267
Hansen E D, Miller T and Chiang T-C 1998 *Phys. Rev. Lett.* **80** 1766
[28] Papaconstantopoulos D A 1986 *Handbook of the Band Structure of Elemental Solids* (New York: Plenum)
[29] Ortega J E and Himpsel F J 1992 *Phys. Rev. Lett.* **69** 844
[30] Kawakami R K *et al* 1998 *Phys. Rev. Lett.* **80** 1754
Kawakami R K *et al* 1999 *Phys. Rev. Lett.* **82** 4098
[31] Luh D-A *et al* 2000 *Phys. Rev. Lett.* **84** 3410
[32] Kawakami R K *et al* 1999 *Nature* **398** 132
[33] Himpsel F J *et al* 1998 *Adv. Phys.* **47** 511
[34] An J M *et al* 2003 *Phys. Rev.* B **68** 045419
[35] Hirayama Y *et al* 1994 *J. Appl. Phys.* **75** 5903
[36] Ohnishi S, Fu C L and Freeman A J 1985 *J. Magn. Magn. Mater.* **50** 161
Rau C *et al* 1986 *Phys. Rev. Lett.* **57** 2311